Developmental Cell
Short Article

Myosin II Dynamics Are Regulated by Tension in Intercalating Cells

Rodrigo Fernandez-Gonzalez,[1] Sérgio de Matos Simoes,[1] Jens-Christian Röper,[2] Suzanne Eaton,[2] and Jennifer A. Zallen[1,*]
[1]Howard Hughes Medical Institute, Developmental Biology Program, Sloan-Kettering Institute, 1275 York Avenue, New York, NY 10065 USA
[2]Max Planck Institute of Molecular Cell Biology and Genetics, Pfotenhauer Strasse 108, 01307 Dresden, Germany
*Correspondence: zallenj@mskcc.org
DOI 10.1016/j.devcel.2009.09.003

SUMMARY

Axis elongation in *Drosophila* occurs through polarized cell rearrangements driven by actomyosin contractility. Myosin II promotes neighbor exchange through the contraction of single cell boundaries, while the contraction of myosin II structures spanning multiple pairs of cells leads to rosette formation. Here we show that multicellular actomyosin cables form at a higher frequency than expected by chance, indicating that cable assembly is an active process. Multicellular cables are sites of increased mechanical tension as measured by laser ablation. Fluorescence recovery after photobleaching experiments show that myosin II is stabilized at the cortex in regions of increased tension. Myosin II is recruited in response to an ectopic force and relieving tension leads to a rapid loss of myosin, indicating that tension is necessary and sufficient for cortical myosin localization. These results demonstrate that myosin II dynamics are regulated by tension in a positive feedback loop that leads to multicellular actomyosin cable formation and efficient tissue elongation.

INTRODUCTION

Morphogenesis involves a combination of biochemical signaling pathways and the translation of these signals into the forces that move cells. Mechanical force is increasingly appreciated as an input that can regulate cell behavior (Gorfinkiel et al., 2009; Solon et al., 2009). Forces acting between cells and tissues regulate gene expression, cell division, and tumor cell progression (Orr et al., 2006; Wozniak and Chen, 2009). A primary source of force generation is actin-based contractility mediated by the myosin II motor protein. Localized actomyosin contractility is required for cell division and migration (Robinson and Spudich, 2004), and patterned myosin II activation at the tissue level can lead to structural transformations such as grooves, tubes, and placodes in multicellular epithelia (Dawes-Hoang et al., 2005; Escudero et al., 2007; Nishimura et al., 2007).

In the *Drosophila* embryo, polarized actomyosin contractility in the plane of the tissue drives the cell rearrangements that elongate the body axis (Irvine and Wieschaus, 1994; Zallen and Wieschaus, 2004; Butler et al., 2009). Actomyosin contractility promotes local neighbor exchange through the contraction of single cell boundaries (Bertet et al., 2004), and the contraction of actomyosin structures spanning multiple pairs of cells leads to the formation of rosettes (Blankenship et al., 2006). Actomyosin organization into multicellular cable-like structures has been implicated in epithelial advance (Franke et al. 2005), compartment boundary formation (Major and Irvine, 2006), and wound healing (Wood et al., 2002), and can occur in response to a variety of signaling pathways (Escudero et al., 2007; Nishimura et al., 2007). However, the cell biological mechanisms that regulate actomyosin cable formation are not well understood.

Here, we show that actomyosin cables in intercalating cells of the *Drosophila* embryo form at a higher frequency than expected by chance, and multicellular contractile structures sustain increased tension as measured by laser ablation. Cell boundaries under increased tension have higher levels of myosin and a lower rate of myosin dissociation from the cortex. An ectopic force is sufficient to recruit myosin and, conversely, relieving tension leads to loss of myosin from the cortex. These results indicate that myosin II localization is stabilized by tension in a mechanism that leads to higher order actomyosin cable formation and efficient tissue elongation.

RESULTS

Myosin II Forms Multicellular Cable-like Structures in Intercalating Cells

Myosin II directs polarized cell rearrangements in the *Drosophila* embryo through the contraction of specific boundaries between cells (Figures 1A–1D) (Bertet et al., 2004; Zallen and Wieschaus, 2004). Time-lapse imaging shows that adjacent myosin-positive edges often contract simultaneously (Figure 1D; see Movie S1 available online). Contraction of these structures leads to multicellular rosettes that form predominantly during the period of rapid intercalation in stage 8 (Figure 1E, blue line) (Blankenship et al., 2006). This may explain why rosettes were overlooked in previous studies at stage 7, when the germband has only reached one-third of its final length (Bertet et al., 2004; Rauzi et al., 2008).

Multicellular contractile structures presumably represent intracellular myosin filaments that are functionally associated across cell boundaries through connections mediated by adherens junctions. These structures are referred to here as actomyosin cables. Actomyosin cables appear to represent sites of

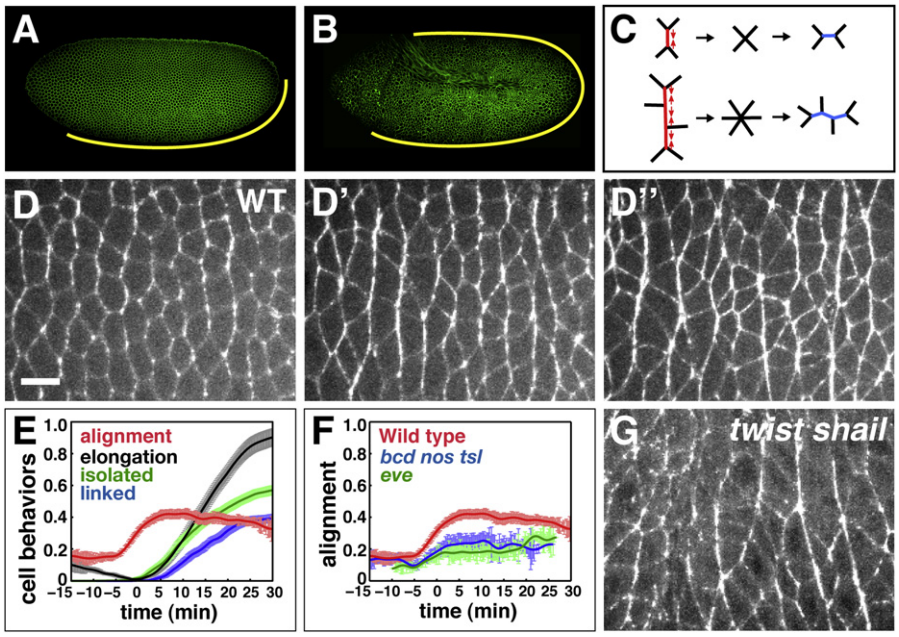

Figure 1. Multicellular Alignment and Formation of Myosin II Cable-like Structures in Intercalating Cells

(A and B) Wild-type embryos before (A) or after (B) elongation of the germband (yellow line).

(C) Contraction of isolated AP edges (top) leads to local neighbor exchange, and contraction of linked AP edges (bottom) leads to multicellular rosette formation.

(D) Confocal images from a time-lapse movie of germband cells expressing Myo:GFP before (D) and 5 min (D′) or 10 min (D″) after the onset of elongation. Anterior left, dorsal up. Scale bar = 10 μm.

(E) Alignment (red) shows the fraction of AP edges (edges oriented at 75°–105° relative to the AP axis) connected to at least one other AP edge (n = 14 embryos). The increase in alignment preceded tissue elongation (black line, the AP length of a group of cells normalized to the length at t = 0 minus 1). The cumulative fraction of isolated (green) or linked (blue) shrinking edges is shown (n = 10 embryos). t = 0 indicates the onset of elongation. Error bars show standard error of the mean in all figures.

(F) Alignment was reduced in embryos mutant for *bcd nos tsl* (blue, n = 5) ($p = 5.0 \times 10^{-4}$) or *eve* (green, n = 3) ($p = 8.6 \times 10^{-4}$) compared to wild-type (red).

(G) Localization of Myo:GFP in a *twist snail* mutant embryo. Anterior, left; dorsal, up.

increased tension, as cell boundaries in cables were aligned perpendicular to the anterior-posterior (AP) axis (Figure 1D). We quantified the extent of alignment in living embryos using a computer algorithm to identify cell boundaries in confocal images (Experimental Procedures). Alignment was measured as the fraction of AP edges (cell-cell interfaces oriented at 75–105° relative to the AP axis) that were directly connected to at least one other AP edge. Wild-type embryos displayed a sharp increase in alignment at the onset of intercalation that plateaued at ~40% of all AP edges (Figure 1E). Embryos zygotically mutant for *eve* or maternally mutant for *bcd, nos*, and *tsl* are defective for elongation and showed significantly reduced alignment (Figure 1F), while alignment occurred normally in *twist snail* mutants that fail to generate mesoderm but are able to elongate (Figure 1G; 45% ± 3% of edges were aligned in *twist snail* at stage 8, n = 3 embryos, compared to 40% ± 2% in wild type). These results indicate that the timing of alignment correlates with intercalary behavior and does not require external forces from the ventral furrow.

The spatial distribution of myosin II was analyzed in time-lapse movies of living embryos that express fluorescently-tagged myosin regulatory light chain from its endogenous promoter (Myo:mCherry, Martin et al., 2008). Myo:mCherry localized predominantly to interfaces between anterior and posterior cells (Figures 2A and 2B). One-third of all AP edges were myosin-positive (39% ± 2%, n = 2609 AP edges in 5 embryos), and nearly two-thirds of the myosin-positive edges were associated with multicellular cables (62% ± 2%) (Figures 2C–2E). Analysis of single-edge behaviors over time revealed that alignment often precedes asymmetric myosin redistribution (Figures S1A and S1B).

The organization of myosin into multicellular cables could arise randomly from independent and unrelated single-cell events. Alternatively, cables could form through a mechanism that actively promotes the accumulation of myosin in adjacent cells. To distinguish between these possibilities, we used statistical methods to calculate the probability that myosin-positive cell edges would be connected by chance. Monte Carlo methods (Fernandez-Gonzalez et al., 2005) were used to simulate random distributions of myosin in the endogenous cellular sheet using the same number of edges that were myosin-positive in vivo. Simulations were repeated 20,000 times for each image (25 images in 5 embryos, 5 time points/embryo). To recapitulate myosin planar polarity, myosin was assigned to edges oriented at 60-120° relative to the AP axis, a restriction that includes a majority of myosin-positive edges in vivo (Figures S2A–S2C).

In contrast to the association of myosin-positive edges with cables in random simulations (44 ± 0.02%), the distribution

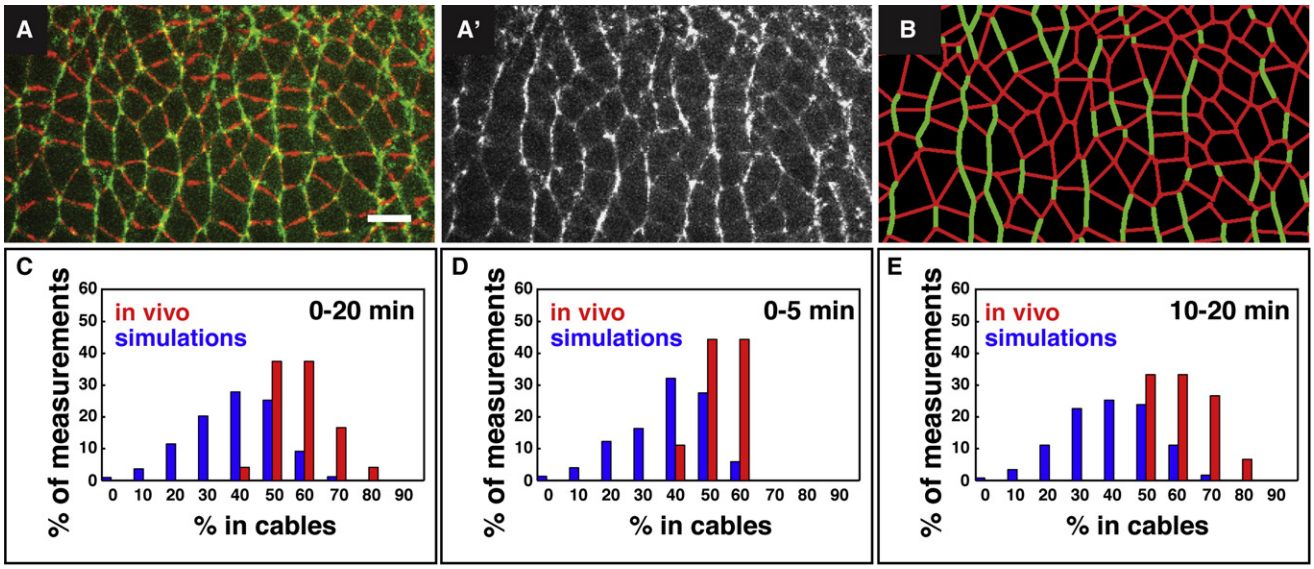

Figure 2. Myosin II Distribution Is Nonrandom in Intercalating Cells

(A) Wild-type embryo expressing Baz:GFP (red) and Myo:mCherry (green, single channel in A′). Anterior, left; dorsal, up. Scale bar = 10 μm.

(B) Quantitation of myosin intensity. Edges were scored as myosin-positive (green) if they had a mean pixel intensity $I \geq 1.15$ relative to DV edges and were oriented at 60°–120° relative to the AP axis.

(C–E) Myosin distributions in vivo (red, n = 5788 edges in 5 embryos) were not recapitulated in Monte Carlo simulations (blue, n = 500,000 simulations). Data shown are for (C) all time points ($p = 2.0 \times 10^{-8}$), (D) stage 7 (t = 0–5 min) ($p = 4.6 \times 10^{-3}$), and (E) stage 8 (t = 10–20 min) ($p = 4.8 \times 10^{-6}$).

of myosin II was significantly more clustered in vivo (Figures 2C–2E) (62 ± 2%, $p = 2.0 \times 10^{-8}$). Similar results were obtained at a range of threshold values for scoring edges as myosin positive (Figures S2D–S2F). These results demonstrate that myosin II is preferentially associated with multicellular contractile structures in intercalating cells.

Actomyosin Cables Display Distinct Mechanical Properties

The nonrandom organization of myosin II into multicellular structures suggests that actomyosin cable formation is actively regulated. To ask if actomyosin cables display distinct mechanical properties, we performed laser ablation of individual boundaries between cells. A 365 nm UV laser was focused on an ~1 μm diameter junctional region labeled with E-cadherin:GFP. This is predicted to sever the plasma membrane and cortical cytoskeleton on both sides of the cell-cell interface (Farhadifar et al., 2007).

Laser ablation induced a local relaxation of cortical tension and an increase in the distance between the vertices attached to the ablated edge (Figure 3; Movies S2–S4). AP edges displayed a greater response to ablation than DV edges (Figures 3A–3C and 3G; Movies S2–S4), consistent with previous studies (Rauzi et al., 2008) and with the planar polarized distribution of myosin II (Zallen and Wieschaus, 2004). The response to ablation was abolished by injecting the Rho-kinase inhibitor Y-27632 (Figures 3D, 3E, and 3H), a drug that blocks myosin cortical localization (Figures S1C and S1D) and arrests germband extension (Bertet et al., 2004). These results indicate that myosin contractility, and not membrane integrity per se, is required for net axial forces between cells in the germband. Conversely, increasing myosin activity by injecting Calyculin A, a serine/threonine phosphatase inhibitor that acts on myosin phosphatase (Ishihara et al., 1989) and leads to increased myosin at the cortex (Figure S1E), converted the mechanical properties of DV edges into those of AP edges (Figures 3F and 3H). These results indicate that differences in myosin II activity are responsible for the differences in tension at AP and DV cell boundaries.

Linked edges associated with multicellular cables displayed a significantly stronger response to ablation than isolated contractile edges (Figures 3A and 3B; Movies S2 and S3). These differences were apparent in terms of the distance retracted by the vertices of the ablated edge (Figure 3G, $p = 7.0 \times 10^{-4}$) and the peak retraction velocities (Figure 3H, p = 0.002). The retraction distance after ablation correlated with the length and amount of myosin in the cable rather than the properties of the ablated edge (Figure 3I; Figures S3A–S3F). These results indicate that mechanical properties are influenced by higher-order cellular organization.

Initial retraction velocities after ablation are considered to be proportional to the endogenous forces at cell boundaries (Hutson et al., 2003; Peralta et al., 2007). Estimating the initial velocity as the peak velocity after ablation, the tension at linked AP edges was greater than the tension at isolated AP and DV edges in a ratio of $T_{\text{linked AP}}:T_{\text{isolated AP}}:T_{\text{DV}} = 3.1:1.7:1$ (Figure 3H). In an independent method, we modeled cell boundaries as mechanical equivalent circuits consisting of a spring and dashpot in parallel (Figure 3J; Figures S3G-S3L). This approach can be used to estimate the relaxation time (τ), a measure of local viscoelastic properties, and the asymptotic distance retracted by the vertices attached to the cut edge (D), which is proportional to the tension on the edge when the local viscoelastic properties are homogeneous (Experimental Procedures). Values for τ are constant throughout the tissue (Figure 3J; Figure S3K and S3L). Therefore, on the spatiotemporal scale of vertex recoil,

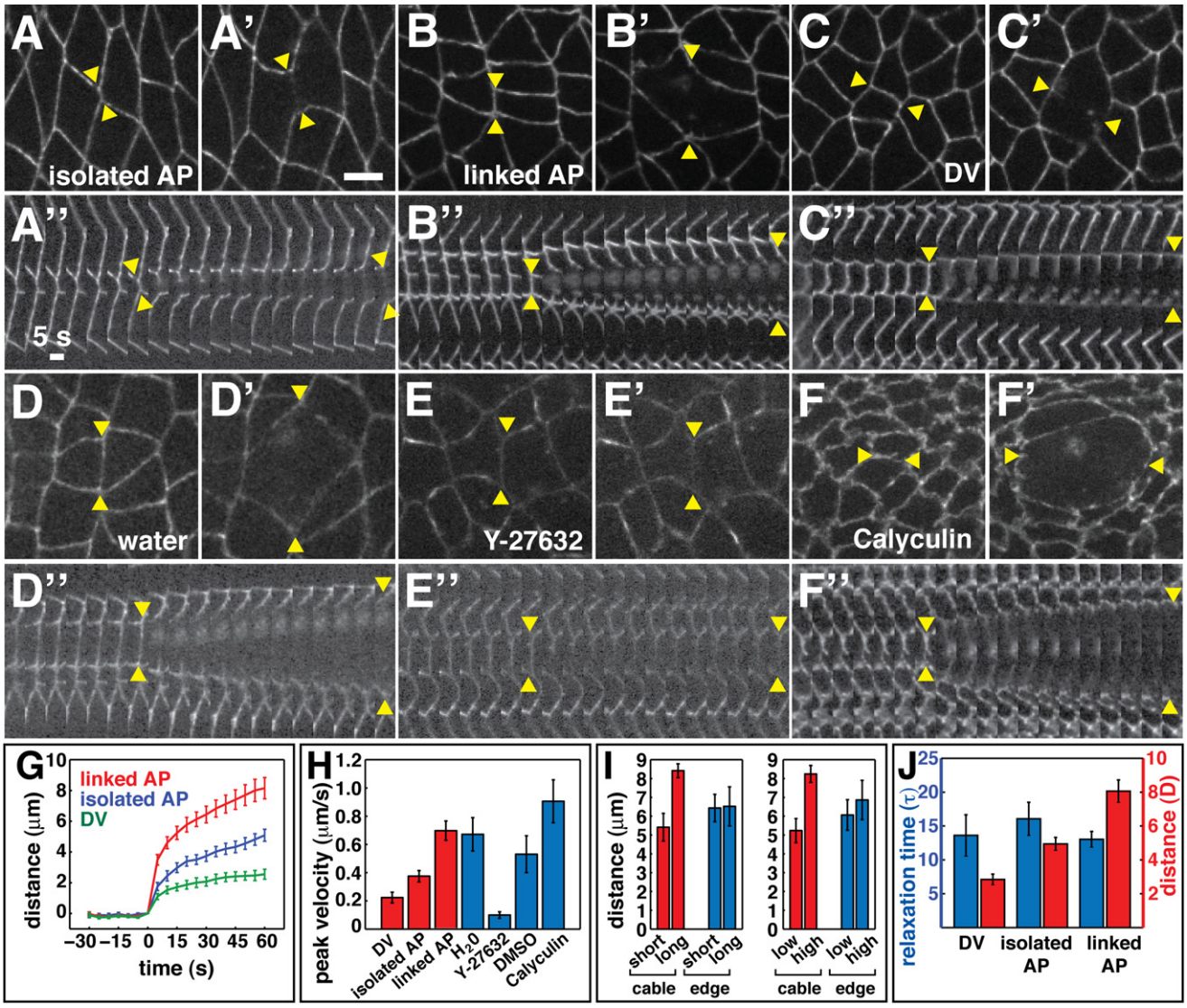

Figure 3. Multicellular Actomyosin Cables Sustain Increased Mechanical Tension

(A–F) Cells expressing E-cadherin:GFP before (A–F) and after (A′–F′) ablation. Arrowheads indicate the vertices attached to the cut edge. Anterior, left; dorsal, up. Scale bar = 5 μm. (A″–F″) Kymographs show vertex displacement over time.

(G–I) Quantitation of laser ablation experiments. (G) The increase in distance between the vertices attached to the cut edge was greater for linked AP edges (red, n = 13) than for isolated AP (blue, n = 10) ($p = 7.0 \times 10^{-4}$) or DV edges (green, n = 11) ($p = 2.9 \times 10^{-6}$). (H) Peak retraction velocities in wild-type uninjected embryos (red bars) were greater for linked AP edges than for isolated AP (p = 0.002) or DV edges ($p = 2.5 \times 10^{-5}$). Peak retraction velocities in injected embryos (blue bars) were lower for AP edges in embryos injected with Y-27632 (n = 8 ablations) compared to water-injected controls (n = 8) (p = 0.0017). Peak retraction velocities were higher for DV edges in embryos injected with Calyculin A (n = 3) compared to DMSO-injected controls (n = 3). Differences in retraction velocities for AP and DV edges in DMSO-injected embryos (1.07 ± 0.10 versus 0.53 ± 0.13 μm/s, p = 0.03) were abolished in Calyculin-injected embryos (0.87 ± 0.19 versus 0.91 ± 0.15 μm/s, p = 0.90). (I) (Left) Retraction distances correlated with the length of the cable (red bars show the 4 shortest and 4 longest cables, p = 0.011), but not with the length of the ablated edge (blue bars show the 4 shortest and 4 longest edges, p = 0.95) (n = 20 ablations). (Right) Retraction distances correlated with the total myosin level in the cable (red bars show the 4 lowest intensity and 4 highest intensity cables, p = 0.008), but not with the level of myosin in the ablated edge (blue bars show the 4 lowest intensity and 4 highest intensity edges, p = 0.57).

(J) Modeling laser ablation data as the recoil of an elastic fiber in a damped environment revealed similar relaxation times in all experiments. The maximum retraction distance was greater for linked AP edges than for isolated AP (p = 0.0022) or DV edges ($p = 9.4 \times 10^{-6}$).

the local viscoelastic properties in the *Drosophila* germband are homogeneous. Values for *D* indicate that the tension at linked AP edges is greater than the tension at isolated AP and DV edges in a ratio of $T_{\text{linked AP}}$:$T_{\text{isolated AP}}$:T_{DV} = 2.8:1.7:1 (Figure 3J), consistent with the peak retraction velocity measurements. These results demonstrate that cortical tension is significantly higher in actomyosin cables than in isolated contractile edges.

These findings contrast with a previous report using an infrared laser (Rauzi et al., 2008). Low-power infrared ablation induces a lesion that is smaller (<0.2 μm) than the lesion induced

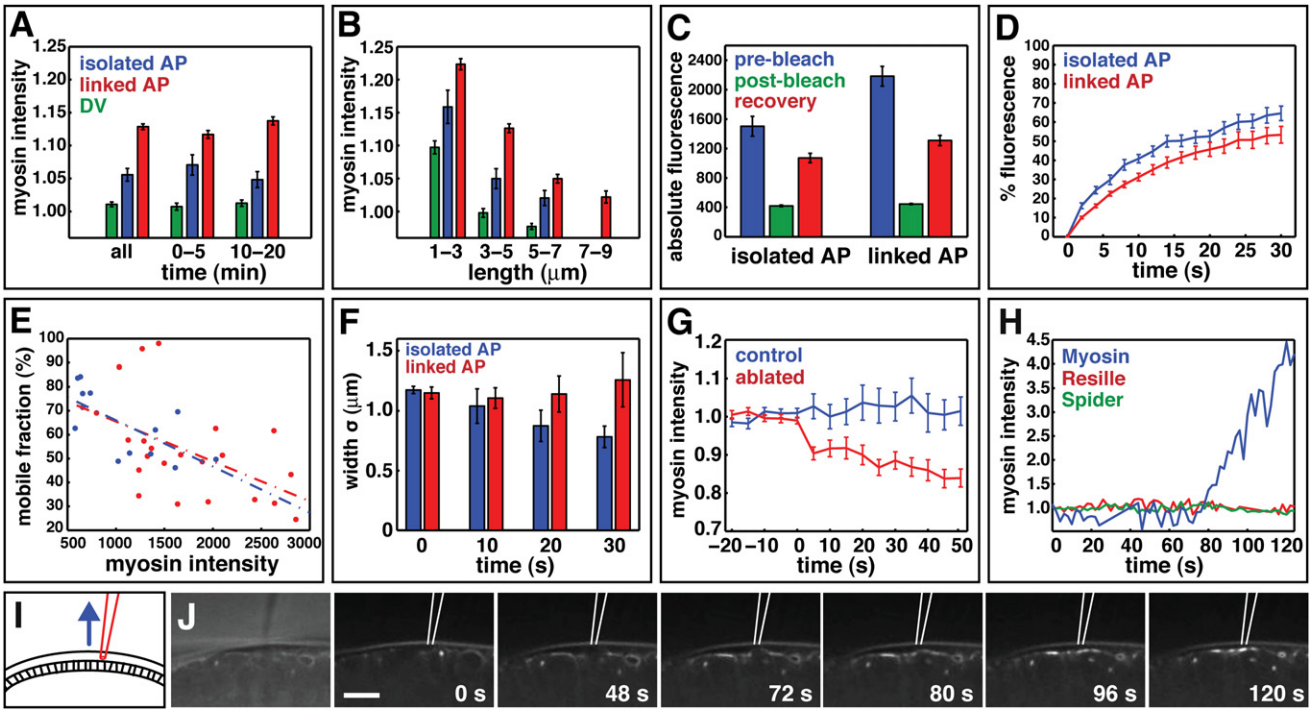

Figure 4. Myosin II Dynamics Are Regulated by Mechanical Tension

(A and B) Myosin II levels in living embryos. (A) Linked AP edges had higher levels of Myo:mCherry than isolated AP edges throughout intercalation (all time points, $p = 2.4 \times 10^{-11}$; t = 0–5 min, p = 0.008; t = 10–20 min, $p = 3.6 \times 10^{-10}$). (B) Linked AP edges had higher levels of Myo:mCherry than isolated AP edges regardless of edge length (p = 0.033, 9.0×10^{-6}, 0.027, 0.0097, for edges with lengths 1-3, 3-5, 5-7 and 7-9 μm). n = 1552 DV, 359 isolated AP, and 2216 linked AP edges in 5 embryos.

(C–F) Myo:GFP is stabilized in linked AP edges. (C) Pre-bleach (blue), post-bleach (green), and post-recovery (red) fluorescence intensities (n = 13 isolated AP, 22 linked AP edges). (D) The percent recovery of pre-bleach fluorescence was reduced for linked AP edges (p = 0.03). (E) The mobile fraction is negatively correlated with pre-bleach fluorescence ($R = -0.60$, $p = 2.0 \times 10^{-4}$). Isolated AP edges, blue dots; linked AP edges, red dots. Dotted lines represent the best linear fits. (F) The width (σ) of the bleached region decreased during fluorescence recovery at isolated AP edges (blue bars, p = 0.0057), but did not change at linked AP edges (red bars, p = 0.65).

(G) Myo:GFP intensity in cables decreased after line ablations (red line, 27 edges) compared to control edges anterior or posterior to the ablated region (blue line, 20 edges) (p = 0.0018). Measurements were normalized to the average fluorescence prior to ablation.

(H–J) Aspiration pressure recruits Myo:GFP to the cortex. (H) Myo:GFP intensity at the cortex relative to fluorescence prior to aspiration for the experiment shown in J (blue line). Resille:GFP (red line) and Spider:GFP (green line) were unaffected by aspiration. (I) A micropipette (red lines) was inserted into the perivitelline space and negative pressure (blue arrow) was applied to deform the apical surface of contacting cells. (J) Cross-sections from a wild-type embryo expressing Myo:GFP. Bright-field image (left) shows the position of the micropipette. Scale bar = 10 μm. t = 0 is the time of aspiration.

by UV ablation in this study (1 μm), and generates retraction velocities that are several times slower (0.11 μm/s versus 0.5 μm/s reported here), suggesting that the infrared ablation experiments only partially disrupt the actomyosin network.

Myosin II Dynamics Are Regulated by Mechanical Tension

Cell intercalation occurs in an epithelial sheet in which forces within cells can trigger mechanotransduction pathways in neighboring cells. If mechanical tension acts as a signal to promote myosin II localization, then myosin levels should be higher at cell boundaries in cables. Consistent with this prediction, we found that linked AP edges had higher levels of myosin II regulatory light chain than isolated AP edges, regardless of stage (Figure 4A) or edge length (Figure 4B). These results demonstrate that cortical myosin levels are increased in multicellular cables.

The accumulation of myosin in cables could occur through an increase in the rate of myosin association or, alternatively, a decrease in the rate of myosin dissociation. To distinguish between these possibilities, we photobleached a 1.0 × 1.4 μm region at the cortex of cells expressing the myosin regulatory light chain fused to GFP (Myo:GFP, Movie S5). Myo:GFP levels immediately after bleaching were similar in all cases (Figure 4C), indicating that photobleaching was complete. Myo:GFP recovered to more than half of pre-bleach fluorescence levels within 30 s (Figure 4D). The rate of recovery was similar for isolated and linked AP edges (Figure S4E), indicating that tension does not affect the rate of myosin recruitment to the cortex. By contrast, the mobile fraction was significantly lower for linked AP edges in cables than for isolated AP edges (Figure 4D, p = 0.03). The mobile fraction decreased dramatically from >75% at edges with low levels of myosin to <40% at edges with high levels of myosin (Figure 4E, $p = 2.0 \times 10^{-4}$). These results suggest that myosin II dissociation from the cortex is inhibited in cortical domains with increased contractile activity.

These results indicate that increased tension correlates with decreased myosin II dissociation from the cortex, resulting in the stabilization of cortical myosin II. Inhibition of myosin dissociation could occur through a reduction in lateral diffusion along the membrane or decreased exchange of protein with the cytoplasm. The extent of lateral diffusion can be measured by quantifying the shape of myosin intensity profiles during fluorescence recovery after photobleaching (Figure 4F). If lateral diffusion contributes to the recovery of fluorescence, then the width of the bleached region should change over time (de Beco et al. 2009). We approximated the width of the bleached region as the standard deviation (σ) of a Gaussian curve fit to the observed intensity profile (Figures S4A–S4D). The width of the bleached region decreased significantly during the recovery of fluorescence at isolated AP edges ($p = 0.0057$) but was constant for recovery at linked AP edges (Figure 4F, $p = 0.65$). The stabilization of myosin cortical localization by tension therefore occurs in part through an inhibition of lateral diffusion.

These results demonstrate that myosin dynamics are not uniform in intercalating populations but instead correlate with local differences in mechanical tension. To ask if tension is necessary for myosin cortical localization, we performed ablations in embryos expressing Myo:GFP. Single-edge ablations led to a significant loss of myosin II in the unablated cortical regions of the affected cells (Figure S4F). To relieve tension at a greater distance from the ablation site, we ablated an ~50 μm line parallel to the AP axis. Line ablations led to a significant decrease in myosin intensity in the intact edges of ablated cables, while myosin intensity outside the ablated region was unaffected (Figure 4G, $n = 27$ ablations, $p = 0.0018$). These results demonstrate that tension is necessary for cortical myosin II localization in intercalating cells.

Conversely, we asked if tension is sufficient for cortical myosin localization using a micropipette aspiration approach to introduce ectopic forces in intercalating cells. Myo:GFP was rapidly recruited to the apical surface in response to microaspiration (Figures 4H–4J) (13/17 experiments). By contrast, two control GFP markers were not affected by microaspiration (Figure 4H) (0/10 Resille:GFP; 0/5 Spider:GFP). The pressure applied in microaspiration experiments was estimated to be 0.15 nN/μm^2 –0.4 nN/μm^2, corresponding to applied forces of 1–3 nN (Experimental Procedures). These values are similar to the forces required to recruit myosin in Dictyostelium (8–15 nN; Effler et al., 2006) and lower than the forces required to induce Twist transcription in *Drosophila* (60 ± 20 nN; Desprat et al., 2008). Together, these results indicate that mechanical tension is necessary and sufficient for myosin cortical localization in intercalating cells.

DISCUSSION

A major challenge in developmental biology is to understand how cell behavior and cytoskeletal activity are coordinated to produce higher order tissue organization. Here, we provide evidence that myosin II is organized into multicellular contractile structures that form nonrandomly in intercalating cells and sustain increased mechanical tension. Mechanical tension is sufficient to promote cortical myosin localization, and conversely, relieving tension leads to a rapid decrease in cortical myosin. These studies demonstrate that myosin II not only generates tension, but myosin II dynamics can also be regulated by tension, generating a positive feedback loop that allows cells to dynamically respond to changes in their mechanical environment.

External forces have been shown to recruit myosin to the cortex during cell division and apical constriction (Effler et al., 2006; Pouille et al., 2009). In intercalating cells, myosin is distributed in a planar polarized fashion in response to striped patterns of gene expression that concentrate contractile proteins in specific cortical domains (Zallen and Wieschaus, 2004). We propose that the recruitment of myosin by tension amplifies these initial subtle asymmetries, reinforcing contractile activity and increasing the number of cells engaged in contractile behavior. This positive feedback loop could explain the formation of multicellular actomyosin cables that promote rosette formation and efficient tissue elongation (Blankenship et al., 2006).

How is mechanical tension translated into myosin II stabilization at the cortex? Evidence from the literature suggests three models of mechanotransduction (Vogel and Sheetz, 2006). First, forces have been shown to influence gene expression in normal cells as well as during tumorigenesis (Orr et al., 2006; Wozniak and Chen, 2009), suggesting that tension could lead to changes in the expression of myosin II regulatory proteins. Tension has been shown to promote β-catenin-dependent expression of Twist (Farge, 2003; Desprat et al., 2008), a transcription factor that regulates apical myosin localization (Dawes-Hoang et al., 2005). However, the rapid recruitment of myosin in response to ectopic forces in intercalating cells suggests that the effect of tension is likely to be independent of transcription. A second possibility is that increased tension at the plasma membrane could alter the trafficking of secreted signaling proteins. Such a mechanism has been proposed to occur during *Drosophila* mesoderm invagination, in which mechanical tension potentiates the activity of the secreted Twist target gene Fog (Pouille et al., 2009). However, Twist and Fog are not expressed or required in intercalating cells, suggesting that myosin localization during intercalation occurs through a different mechanism. Finally, mechanical tension can alter signaling pathways directly through force-dependent changes in protein interactions (Sawada et al., 2006; del Rio et al., 2009). Myosin itself could act as the mechanosensor in this context, as tension favors the ADP-bound form of myosin II in vitro, stabilizing its association with actin (Cremo and Geeves, 1998; Veigel et al., 2003; Kovács et al., 2007). Mechanical tension alters the activity of several myosin and kinesin motors and may represent a general mechanism regulating motor protein function (Spudich, 2006; Kee and Robinson, 2008).

Multicellular actomyosin cables are characteristic of many developmental processes including epithelial closure (Franke et al., 2005; Solon et al., 2009), tracheal tube invagination (Nishimura et al., 2007), and neural plate bending and elongation (Nishimura and Takeichi, 2008). The role of mechanical tension in regulating myosin dynamics could serve to promote contractile activity and maintain the integrity of contractile cables in the presence of interruptions caused by cell shape changes, cell division, or cell death. In the *Drosophila* embryo, spatially regulated mechanical forces may also act as a long-range signal to allow cells to maintain planar polarity despite the transient nature of local cell interactions during morphogenesis.

EXPERIMENTAL PROCEDURES

Time-Lapse Imaging

Embryos were dechorionated in 50% bleach for 2 min, washed with water, and mounted in halocarbon oil 27 (Sigma) between a coverslip and an oxygen-permeable membrane (YSI). The anterior ventrolateral region of the germband was imaged with an Ultraview RS5 spinning disk confocal (Perkin Elmer) controlled by Metamorph software (Universal Imaging) using a 40× oil-immersion objective (NA 1.3, Zeiss).

Automated Image Analysis

We developed a computer algorithm in Matlab (Mathworks)/DIPImage (TU Delft) for automated identification of cell outlines in confocal images. An independent algorithm was used to track cell behavior in Figure 1E (Ori Weitz and J.A.Z., unpublished data). Myosin intensity (I_{edge}) was measured as the average Myo:mCherry intensity within a 3 pixel (1 μm) wide mask corresponding to a single interface. To account for variations in image intensity, myosin intensity (I) for each edge was calculated as:

$$I = \frac{I_{edge} - I_{background}}{I_{DV}}$$

where I_{DV} was the average intensity of the ten closest DV edges and $I_{background}$ was the average pixel value outside the embryo.

Laser Ablation

Dechorionated embryos were mounted in halocarbon oil 700 (Sigma) and imaged with an Ultraview RS5 spinning disk confocal (Perkin Elmer). An N_2 Micropoint laser (Photonics Instruments) tuned to 365 nm was used to ablate cell interfaces labeled with *E-cadherin:GFP* or *Myo:GFP*. Imaging was performed before and after ablation using a 63× oil immersion lens (NA 1.4, Zeiss) that was also used to focus the Micropoint laser. All vertices in the field were identified and tracked using the segmentation algorithm above. Edges responded similarly to ablation whether identified by orientation or myosin intensity.

Drug Injection

Pharmacological inhibitors were injected ventrally into the perivitelline space of embryos at stage 7 or stage 8. Rho-kinase inhibitor (Y-27632 dihydrochloride, Tocris Bioscience) was injected at 100 mM. Calyculin A (Sigma) was injected at 1 μM. Injected solutions are diluted ~50-fold in the embryo.

Microaspiration

Dechorionated embryos were lined up on an agarose pad and transferred to a coverglass covered with heptane glue. Embryos were dried in a sealed container with silica beads for 6 min and covered with a 1:1 halocarbon oil 27:700 mixture (Sigma). Embryos were imaged with an Ultraview RS5 spinning disk confocal and a 40× oil immersion objective (NA 1.3, Zeiss). A pulled glass micropipette connected to a manual piston pump (CellTram Air, Eppendorf AG) was mounted in a micromanipulator on the microscope stage. The micropipette tip was broken against a coverglass and inserted into the perivitelline space of embryos expressing *sqh-sqh:GFP*, *resille:GFP* or *spider:GFP*. Negative pressure was applied to the micropipette until cell displacement was observed. Insertion of the micropipette occasionally resulted in cell wounding and myosin accumulation prior to the application of negative pressure; these experiments were discarded.

Fluorescence Recovery after Photobleaching

Dechorionated embryos were mounted in halocarbon oil 27 (Sigma) between a coverslip and an oxygen-permeable membrane (YSI). The ventrolateral germband was imaged with an LSM 510 laser scanning confocal (Zeiss) using a 40× oil-immersion objective (NA 1.3, Zeiss) and zoom 4. Embryos expressing *myo:GFP* were imaged at an optical slice thickness of 1.7 μm to include a majority of junctional myosin. A 1.0 μm x 1.4 μm cortical region was photobleached. Fluorescence intensity in the bleached region was measured at each time point using custom Matlab routines. Intensities were background corrected by subtracting the post-bleach fluorescence. Only experiments in which cell boundaries remained in focus throughout the movie were analyzed.

Statistical Analysis

Mean values were compared using Student's t test, with Holm's correction when more than two groups were considered (Glantz, 2002). The variances of multiple data sets were compared using the *F*-test. To compare time curves, the areas under the curves were used as the test statistic. The significance of correlation coefficients was evaluated by transforming the correlation value into a *t* statistic using the Matlab *corrcoef* function (Mathworks). Monte Carlo simulations were carried out for each image by randomly assigning myosin to the same number of edges that were identified as myosin positive in vivo. Only edges with an orientation of 60°–120° were selected to recapitulate myosin planar polarity. The percentage of myosin-positive edges in cables was calculated for each in vivo image or simulation (20,000 simulations/image). The distribution of myosin-positive edges in vivo was compared to the in silico distribution using the Kolmogorov-Smirnov test.

SUPPLEMENTAL DATA

Supplemental data include Supplemental Experimental Procedures, references, four figures, and five movies and can be found online with this article at http://www.cell.com/developmental-cell/supplemental/S1534-5807(09)00385-2/.

ACKNOWLEDGMENTS

We thank Ori Weitz for developing the computational methods for automated cell tracking in Figure 1E. We are grateful to Richard Zallen for valuable input throughout this project and to Dene Farrell, Morgan Reeds, and Justina Sanny for manually correcting segmented movies. We thank Adam Martin and Eric Wieschaus for fly stocks and Kathryn Anderson, Emily Marcinkevicius, Mimi Shirasu-Hiza, Gillian Siegal, Masako Tamada, Athea Vichas, Ori Weitz, Eric Wieschaus, Frederik Wirtz-Peitz, and Richard Zallen for comments on the manuscript. This work was supported by a Burroughs Wellcome Fund Career Award in the Biomedical Sciences, a March of Dimes Basil O'Connor Starter Scholar Award, a Searle Scholar Award, a W.M. Keck Foundation Distinguished Young Scholar in Medical Research Award, and NIH/NIGMS R01 grant GM079340 to J.A.Z. J.A.Z. is an Early Career Scientist of the Howard Hughes Medical Institute.

Received: May 27, 2009
Revised: July 28, 2009
Accepted: September 9, 2009
Published online: October 29, 2009

REFERENCES

Bertet, C., Sulak, L., and Lecuit, T. (2004). Myosin-dependent junction remodelling controls planar cell intercalation and axis elongation. Nature *429*, 667–671.

Blankenship, J., Backovic, S., Sanny, J., Weitz, O., and Zallen, J. (2006). Multicellular rosette formation links planar cell polarity to tissue morphogenesis. Dev. Cell *11*, 459–470.

Butler, L.C., Blanchard, G.B., Kabla, A.J., Lawrence, N.J., Welchman, D.P., Mahadevan, L., Adams, R.J., and Sanson, B. (2009). Cell shape changes indicate a role for extrinsic tensile forces in Drosophila germ-band extension. Nat. Cell Biol. *11*, 859–864.

Cremo, C., and Geeves, M. (1998). Interaction of actin and ADP with the head domain of smooth muscle myosin: implications for strain-dependent ADP release in smooth muscle. Biochemistry *37*, 1969–1978.

Dawes-Hoang, R., Parmar, K., Christiansen, A., Phelps, C., Brand, A., and Wieschaus, E. (2005). folded gastrulation, cell shape change and the control of myosin localization. Development *132*, 4165–4178.

de Beco, S., Gueudry, C., Amblard, F., and Coscoy, S. (2009). Endocytosis is required for E-cadherin redistribution at mature adherens junctions. Proc. Natl. Acad. Sci. USA *106*, 7010–7015.

del Rio, A., Perez-Jimenez, R., Liu, R., Roca-Cusachs, P., Fernandez, J., and Sheetz, M. (2009). Stretching single talin rod molecules activates vinculin binding. Science *323*, 638–641.

Desprat, N., Supatto, W., Pouille, P., Beaurepaire, E., and Farge, E. (2008). Tissue deformation modulates twist expression to determine anterior midgut differentiation in Drosophila embryos. Dev. Cell *15*, 470–477.

Effler, J., Kee, Y., Berk, J., Tran, M., Iglesias, P., and Robinson, D. (2006). Mitosis-specific mechanosensing and contractile-protein redistribution control cell shape. Curr. Biol. *16*, 1962–1967.

Escudero, L., Bischoff, M., and Freeman, M. (2007). Myosin II regulates complex cellular arrangement and epithelial architecture in Drosophila. Dev. Cell *13*, 717–729.

Farge, E. (2003). Mechanical induction of Twist in the Drosophila foregut/stomodeal primordium. Curr. Biol. *13*, 1365–1377.

Farhadifar, R., Roper, J.C., Aigouy, B., Eaton, S., and Julicher, F. (2007). The influence of cell mechanics, cell-cell interactions, and proliferation on epithelial packing. Curr. Biol. *17*, 2095–2104.

Fernandez-Gonzalez, R., Barcellos-Hoff, M., and Ortiz-de-Solorzano, C. (2005). A tool for the quantitative spatial analysis of complex cellular systems. IEEE Trans. Image Process. *14*, 1300–1313.

Franke, J., Montague, R., and Kiehart, D. (2005). Nonmuscle myosin II generates forces that transmit tension and drive contraction in multiple tissues during dorsal closure. Curr. Biol. *15*, 2208–2221.

Glantz, S. (2002). Primer of Biostatistics (New York: McGraw-Hill).

Gorfinkiel, N., Blanchard, G., Adams, R., and Martinez Arias, A. (2009). Mechanical control of global cell behaviour during dorsal closure in Drosophila. Development *136*, 1889–1898.

Hutson, M., Tokutake, Y., Chang, M., Bloor, J., Venakides, S., Kiehart, D., and Edwards, G. (2003). Forces for morphogenesis investigated with laser microsurgery and quantitative modeling. Science *300*, 145–149.

Irvine, K., and Wieschaus, E. (1994). Cell intercalation during Drosophila germband extension and its regulation by pair-rule segmentation genes. Development *120*, 827–841.

Ishihara, H., Martin, B., Brautigan, D., Karaki, H., Ozaki, H., Kato, Y., Fusetani, N., Watabe, S., Hashimoto, K., and Uemura, D. (1989). Calyculin A and okadaic acid: inhibitors of protein phosphatase activity. Biochem. Biophys. Res. Commun. *159*, 871–877.

Kee, Y., and Robinson, D. (2008). Motor proteins: myosin mechanosensors. Curr. Biol. *18*, R860–R862.

Kovács, M., Thirumurugan, K., Knight, P., and Sellers, J. (2007). Load-dependent mechanism of nonmuscle myosin 2. Proc. Natl. Acad. Sci. USA *104*, 9994–9999.

Major, R., and Irvine, K. (2006). Localization and requirement for Myosin II at the dorsal-ventral compartment boundary of the Drosophila wing. Dev. Dyn. *235*, 3051–3058.

Martin, A., Kaschube, M., and Wieschaus, E. (2008). Pulsed contractions of an actin-myosin network drive apical constriction. Nature *457*, 495–499.

Nishimura, T., and Takeichi, M. (2008). Shroom3-mediated recruitment of Rho kinases to the apical cell junctions regulates epithelial and neuroepithelial planar remodeling. Development *135*, 1493–1502.

Nishimura, M., Inoue, Y., and Hayashi, S. (2007). A wave of EGFR signaling determines cell alignment and intercalation in the Drosophila tracheal placode. Development *134*, 4273–4282.

Orr, A., Helmke, B., Blackman, B., and Schwartz, M. (2006). Mechanisms of mechanotransduction. Dev. Cell *10*, 11–20.

Peralta, X., Toyama, Y., Hutson, M., Montague, R., Venakides, S., Kiehart, D., and Edwards, G. (2007). Upregulation of forces and morphogenic asymmetries in dorsal closure during Drosophila development. Biophys. J. *92*, 2583–2596.

Pouille, P., Ahmadi, P., Brunet, A., and Farge, E. (2009). Mechanical signals trigger Myosin II redistribution and mesoderm invagination in Drosophila embryos. Sci Signal *2*, ra16.

Rauzi, M., Verant, P., Lecuit, T., and Lenne, P. (2008). Nature and anisotropy of cortical forces orienting Drosophila tissue morphogenesis. Nat. Cell Biol. *10*, 1401–1410.

Robinson, D., and Spudich, J. (2004). Mechanics and regulation of cytokinesis. Curr. Opin. Cell Biol. *16*, 182–188.

Sawada, Y., Tamada, M., Dubin-Thaler, B., Cherniavskaya, O., Sakai, R., Tanaka, S., and Sheetz, M. (2006). Force sensing by mechanical extension of the Src family kinase substrate p130Cas. Cell *127*, 1015–1026.

Solon, J., Kaya-Copur, A., Colombelli, J., and Brunner, D. (2009). Pulsed forces timed by a ratchet-like mechanism drive directed tissue movement during dorsal closure. Cell *137*, 1331–1342.

Spudich, J. (2006). Molecular motors take tension in stride. Cell *126*, 242–244.

Veigel, C., Molloy, J., Schmitz, S., and Kendrick-Jones, J. (2003). Load-dependent kinetics of force production by smooth muscle myosin measured with optical tweezers. Nat. Cell Biol. *5*, 980–986.

Vogel, V., and Sheetz, M. (2006). Local force and geometry sensing regulate cell functions. Nat. Rev. Mol. Cell Biol. *7*, 265–275.

Wood, W., Jacinto, A., Grose, R., Woolner, S., Gale, J., Wilson, C., and Martin, P. (2002). Wound healing recapitulates morphogenesis in Drosophila embryos. Nat. Cell Biol. *4*, 907–912.

Wozniak, M.A., and Chen, C.S. (2009). Mechanotransduction in development: a growing role for contractility. Nat. Rev. Mol. Cell Biol. *10*, 34–43.

Zallen, J., and Wieschaus, E. (2004). Patterned gene expression directs bipolar planar polarity in Drosophila. Dev. Cell *6*, 343–355.